ORIGINAL RESEARCH ARTICLE Civil Engineering in Transport D71



This is an open access article distributed under the terms of the Creative Commons Attribution 4.0 International License (CC BY 4.0), which permits use, distribution, and reproduction in any medium, provided the original publication is properly cited. No use, distribution or reproduction is permitted which does not comply with these terms.

MECHANICAL PROPERTIES INVESTIGATION AND OPTIMIZATION OF AMBIENTLY CURED ALKALI-ACTIVATED CONCRETE

Kothoju Saibaba*, B. Kondraivendhan

Department of Civil Engineering, SVNIT, Surat, Gujarat, India

*E-mail of corresponding author: d16am012@amd.svnit.ac.in

Kothoju Saibaba © 0000-0001-7115-2800,

B. Kondraivendhan 0 0000-0002-1589-919X

Resume

The mechanical, microstructural and statical interpretation of the Alkali Activated Concrete (AAC), prepared using fly ash with crushed granulated corex slag as the binder ingredient, are examined in this work. Here, cast in-situ alkali-activated concrete strengths and substitute slag concentrations of 0-50% by fly-ash weight were undertaken to determine a workable manufacturing process and were all considered for up to 28 days. Moreover, in microstructural research, C-A-S-H gel is produced by adding Ground Granulated Corex Slag (GGCS) to the binder-generated structural changes in the in-situ alkali-activated concrete. As a result, this research obtained perfect mixture fractions by synthesizing 25% GGCS with 0.4% of the liquid-to-binder ratio, in addition, a unified desirability of 80% was attained.

Article info

Received 15 December 2022 Accepted 10 March 2023 Online 19 April 2023

Keywords:

fly-ash ground granulated corex slag (GGCS) alkali-activated slag-concrete (AASC) response surface mechanical properties microstructural analysis

ISSN 1335-4205 (print version) ISSN 2585-7878 (online version)

Available online: https://doi.org/10.26552/com.C.2023.044

1 Introduction

Concrete use is expanding quickly due to the rising industrialization and housing need. The majority of infrastructure is presently built with concrete. Ordinary Portland Cement (OPC) is a vital element when making conventional concrete. The only additional material used more frequently than concrete on Earth is water [1]. One of the workable solutions for lowering the CO2 emissions has been suggested as creation of the low-carbon replacement binders [2]. An OPC binder can be replaced with geopolymer, a green substance that is ecologically friendly and devoid of cement. In an alkaline environment, the silica-alumina pebbles undergo a rapid chemical reaction that results in a 3D polymer sequence with a ring structure containing Si-O-Al-O links [3].

On the other hand, the OPC is not necessary when using alkali-activated concrete. The binder was produced when an aluminosilicate material was subjected to strong alkaline solutions. It is clear that throughout the manufacturing of OPC, enormous volumes of CO2 were released into the atmosphere in addition to depleting natural resources. It is necessary to use a green substitute material to counteract these impacts.

Making environmentally friendly concrete requires using alternative resources [4]. Geopolymer concrete is made by mixing aggregates and residual material with cementing gel geopolymer [5]. Alkali-activated binders generate up to 80% less CO2 than the Portland cement. [6].

Despite having existed since the nineteenth century [7] and possessing several advantageous qualities, the geopolymer system is not as frequently utilized in producing concrete as OPC. Cons of the two-part geopolymer binders have limited their usage in concrete production [8]. Though the technical features of the concrete made with this binder are improved, it may provide extra environmental advantages, as well [9]. It was found that increased ratio of calcium fly ash in concrete provides a compressive strength of 65 MPa without the use of high-temperature curing [10]. The activator, on the other hand, was still fluid, [11]. Creation of an one-part geopolymer mix has been attempted. Their research focused on creating one-part binders suitable from an economic and environmental standpoint, [12].

Burning coal in thermal power plant boilers produces a waste product known as fly ash. Fly ash is mainly

m D72 saibaba, kondraivendhan

composed of alumina with silica, with small amounts of iron oxide, lime and magnesia added for balance. Massive volumes of fly ash are produced due to fast industrialization, as it accumulates over time and poses a risk to the environment. Alumina and silica-carrying components are required for geopolymer reactions and fly ash has attracted the attention of researchers as a relevant resource for geopolymer product development [13]. Fly ash is utilized to create geopolymers to reduce the fly ash's steadily growing environmental effect and protect naturally occurring aluminosilicate minerals [14]. It also offers the advantages of being workable, accessible, mechanically sound and improving end product durability [15]. Fly ash and alkali mix during polymerization create a cementitious substance comprised of alumina-silicate-hydrate (A-S- H) gel [16]. Poor fly ash reactivity has shown to be challenging since it results in a sluggish setting and strength properties. Before the final cemented structure is formed, fly ash is typically only partially broken down [17-18]. Granulated Blast Furnace Slag (GBFS), for example, has been utilized to improve the reactivity of geopolymer precursors, according to [19]. The main constituents of GBFS, which is granular and glassy, include oxides like SiO2, CaO, Al2O3 and MgO. It is created by rapidly cooling molten blast furnace (BF) slag, a by-product of iron manufacturing, often by submersion in water, followed by crushing to improve reactivity. The process causes the Ca in the slag to hydrate, forming C-S-H gel, a cementitious phase that enhances the setting and strength features [20].

Ordinary Portland cement concrete (OPCC) and alkali-activated slag concrete (AASC) have benefits, including improved durability, high strength and minimal environmental effect. Hydrated sodium silicate gel, with crystalline hydrated calcium silicate gel (C-A-S-H or C-S-H), are the primary reaction products of AASC (N-A-S- H). Due to its low CaO/SiO2 ratio and other microstructural changes, the C-S-H gel in AASC varies from that seen in Portland cement concrete [21]. Studies [22-23] have shown that the kind and nature of the starting material Ground Granulated Blast Furnace Slag (GGBFS), the quantity and composition of the alkaline activator solution, as well as the curing conditions, have a significant impact on the mechanical and toughness properties of AASC. Consequently, it is crucial to fully understand a novel type of concrete's mechanical performance and toughness characteristics before using it in a building. To serve as a reliable foundation material for AASC, GGBFS also needs sufficient amounts of calcium and silica with alumina species. When alkali hydroxide or alkali silicate are used as activators separately, rather than both, the strength is lower [24]. Multiple investigations have been conducted on the mechanical strength and robustness characteristics of AASC. It is not easy to find information on how to blend materials for AASC with the appropriate compressive strength [25]. By choosing the right proportions of concrete components from the literature [26-27], it is possible to create alkaliactivated concretes with the requisite strength. Based on its compressive strength, concrete's flexural and split tensile strengths may be estimated using the codified equations [28].

To examine effects, connections the interconnections among dependent variables (responses) and independent elements, the Response Surface Methodology (RSM) links the output outcome to independent variables [29]. The response surface approach has been used to build models and enhance mixes in various academic fields. Several sectors started using statistical design approaches in the 1930s due to Box and Wilson's creation of the response surface procedure in 1951 [9]. The response surface approach is commonly applied in producing conventional OPC and geopolymers to imitate and enhance experimental findings [30].

Davidovits [12], initially utilized RSM to predict the compressive strength of a mixed paper concrete in terms of optimizing the model. The research was backed by several scientists [31] [32-33]. In their recent work [34], hybrid design systems for roller-compacted concrete were created using the RSM approach. They improved the performance of roller-compacted rubber concrete (RCR) mixes and reduced water absorption. By predicting their mechanical and post-cracking behaviour, [35] built and refined engineered geopolymer composites and effectively increased the compressive strength and ductility of the necessary cementitious composites.

In recent research, anhydrous GCS raw materials were converted into one-part alkali-activated binders. However, few researchers have used the RSM approach to develop and predict the behaviour of one-part geopolymer binders manufactured from anhydrous corex slag and supplemented with low calcium fly ash [36]. In the current study, alkali-activated concrete was made and allowed to cure at room temperature and in an oven. It could also be cast in place. The strength and microstructures of cast in-situ alkali-activated concrete were investigated at various Ground Copper Slag (GCS) levels while utilizing the conventional sodium silicate and sodium hydroxide combination. In one section, RSM was used to conduct optimization research on fly ash and GCS parameters to produce the most resilient alkaliactivated concrete.

2 Materials and methods

2.1 Materials

2.1.1 Flyash

Fly ash was the main source of aluminosilicates employed in this experiment's geopolymer binder (ASTM Class F). Ninety-five percent of the fly ash used in this investigation, which had a relative density of 2.2 as well as a mesh size of 45 microns, went through the sieve. Table 1 shows the chemical composition as established by chemical characterization.

2.1.2 Ground granulated Corex slag

This study utilized ground granulated Corex slag as a supplementary binder (GGCS). It is a by-product of the iron industry, which primarily consists of minerals with the chemical composition of calcium aluminosilicate. Owing to its strong reactivity with particular surface area, it was believed that using the GGCS as a fly ash replacement in one-part alkali-activated substances would improve their tensile qualities. Table 1 displays the chemical makeup of the GGCS oxide utilized in this study, with GGCS slag replacing fly ash at weight percentages of 0%, 10%, 20%, 30%, 40% and 50%, respectively.

2.1.3 Alkaline solution

Sodium Hydroxide (NaOH) with sodium silicate (Na $_2$ SiO $_3$) solutions were mixed to produce the activator solution. The 97-98% pure NaOH pellets and tap water were combined to create a sodium hydroxide solution with the right concentration. A local commercial supplier provided sodium silicate solution in the ready-made form.

Composition of Sodium silicate: Color: colourless/White liquid physical state; Density: 1.44: 1.56 g/cm3, Mass percentage: 44:48 of total solids, respectively. The densities of sodium hydroxide and complete alkaline solutions were 1.15 and 1.5 g/cm3, respectively. This investigation used a single alkaline solution with a constant NaOH concentration of 8M.

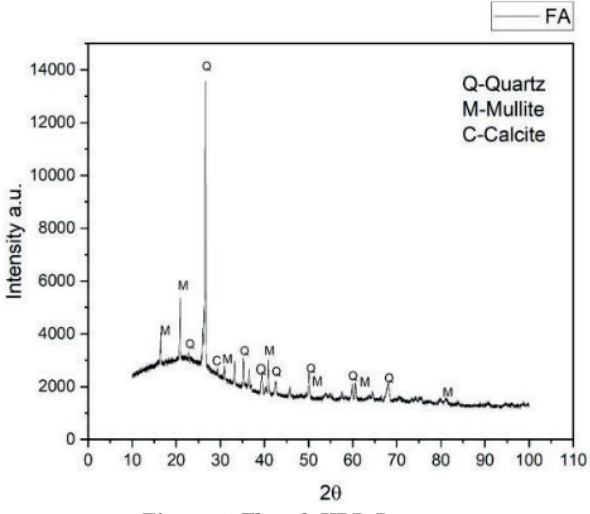


Figure 1 Fly ash XRD Pattern

2.1.4 Aggregates

The coarse aggregate is crushed rock granite, whereas the fine aggregate is local sand, Table 2. For fine and coarse aggregates, the specific gravity and bulk modulus, with void ratio, are 2.52, 1.54 g/cm3, 0.632 and 2.47, 1.678 g/cm3, 0.456. A constant weight ratio of 0.7 was used for coarse aggregate to total aggregate.

Figures 1 and 2 show the fly ash XRD pattern and the Corex slag XRD pattern for the method, respectively, with intensity on the Y-axis and 2θ on the X-axis.

The chemical analysis of GGCS powder and fly ash was carried out using an Inductively coupled plasma optical emission spectrometer Loss on ignition (LOI) was measured by calculating the weight loss upon heating. Instrument used in the present study is Bruker AVANCE III 700 MHz NMR spectrometer equipped with a 5 mm triple resonance cryoprobe with Z-gradient. The phase assemblages of AAMs were generated using the simulated precursors with 80 wt % SiO2 + CaO + Al2O3 as the primary contents, which play the most crucial role during the alkali-activation of aluminosilicate materials.

Table 3 shows the mixed proportions of AASC concrete. Here, L/B denotes the liquid-to-binder ratio, M denotes moles and FA and CA are Fine and Coarse Aggregate. This table gives a detailed explanation of mix designation, Fly ash, corex slag, NaOH and other parameters with their proportions.

2.1.5 Mixing, sample preparation and curing

To create the necessary molarity of sodium hydroxide solution, sodium hydroxide pellets are diluted with water. For example, 255g of sodium hydroxide pellets are dissolving in water to create 1 kilogram of an 8M sodium hydroxide solution. The concentration of the sodium hydroxide solution affects the mass of

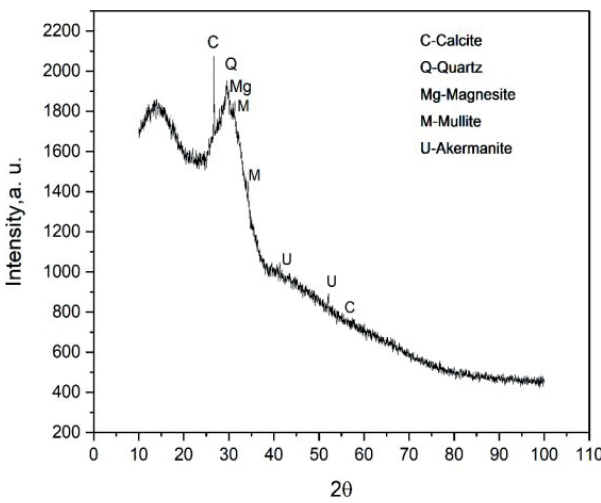


Figure 2 Corex slag XRD Pattern

m D74 saibaba, kondraivendhan

Table 1 Fly ash and GGCS Oxide Compositions

Oxide	Fly ash (Wt. %)	GGCS (Wt. %)
Calcium oxide, CaO	3.62	35.79
$Silicon oxide, SiO_2$	56.38	34.58
Aluminium oxide, ${\rm Al_2O_3}$	23.30	17.28
Iron oxide, Fe_2O_3	15.92	0.92
Magnesium oxide, MgO	0.34	8.05
Potassium oxide, K ₂ O	-	-
Loss of ignition, LOI	0.79	0.97

Table 2 Basic Properties Coarse and Fine Aggregates

Basic Property	Fine Aggregate	Coarse Aggregate
Specific Gravity	2.54	2.78
Water absorption	2%	0.6%
Fineness modulus	2.62	7.28
Bulk density	1.39	1.48

Table 3 Mix Proportions of AASC concrete

Mix designation	Fly ash (kg/ m³)	Corex slag (kg/m³)	L/B ratio	NaOH(kg/ m³)	${ m Na}_2{ m SiO}_3 \ { m (kg/m}^3)$	M	FA (kg/m³)	CA (kg/m³)	$\begin{array}{c} \mathrm{SiO}_{_{2^{/}}} \\ \mathrm{Al}_{_{2}}\mathrm{O}_{_{3}} \end{array}$
A1F100S0	444.45	0	0.35	44.45	111.1	8	540	1260	2.42
A1F90S10	400.00	44.44	0.35	44.45	111.1	8	540	1260	2.38
A1F80S20	355.56	88.89	0.35	44.45	111.1	8	540	1260	2.35
A1F70S30	311.11	133.33	0.35	44.45	111.1	8	540	1260	2.30
A1F60S40	266.69	177.76	0.35	44.45	111.1	8	540	1260	2.30
A1F50S50	222.22	222.22	0.35	44.45	111.1	8	540	1260	2.25
A2F100S0	428.50	0	0.40	49	122.5	8	540	1260	2.42
A2F90S10	385.65	42.85	0.40	49	122.5	8	540	1260	2.38
A2F80S20	342.8	85.70	0.40	49	122.5	8	540	1260	2.35
A2F70S30	299.95	128.55	0.40	49	122.5	8	540	1260	2.30
A2F60S40	257.10	171.40	0.40	49	122.5	8	540	1260	2.30
A2F50S50	214.25	214.25	0.40	49	122.5	8	540	1260	2.25
A3F100S0	413.80	0	0.45	53	133	8	540	1260	2.42
A3F90S10	372.42	41.38	0.45	53	133	8	540	1260	2.38
A3F80S20	331.04	82.76	0.45	53	133	8	540	1260	2.35
A3F70S30	289.66	124.14	0.45	53	133	8	540	1260	2.30
A3F60S40	248.28	165.52	0.45	53	133	8	540	1260	2.30
A3F50S50	206.90	206.90	0.45	53	133	8	540	1260	2.25

sodium hydroxide pellets in the liquid. An amount of 39 g of sodium hydroxide pellets is needed to make a 1M sodium hydroxide solution kilogram. After that, the sodium hydroxide and sodium silicate solutions are blended. The moisture content of the sodium silicate solution is disregarded, while creating sodium hydroxide solution or calculating sodium hydroxide concentration. One day prior to casting, the sodium silicate with sodium hydroxide solutions are adequately combined to achieve ideal solution mixing.

NaOH and Na₂SiO₃ solutions were thoroughly combined in this study's alkaline solution, Na₂SiO₃,

then heated to 25 ± 2 °C 24 hours before usage. The activators' dosages are listed as a percentage of the binder, varying NaOH to (0.35, 0.40 and 0.45). A drum mixer with a saturated dry surface condition thoroughly mixed coarse and fine materials with a binder during dry Mixing. The alkaline liquid was adequately mixed and diluted with water. The two components were then blended for 5 minutes at a temperature of 27 ± 2 °C after combining the dry mixture and liquid combination. Preparing the alkaline solution 24 hours in advance was the major challenge with the Mixing procedure. This issue limits the use of fly ash-based geo-polymer

concrete and makes precast concretes a better fit. The issue of temperature increase during the production of alkaline solutions is another.

After mixing, the cement was poured into concrete molds measuring 150 mm x 150 mm x 150 mm, vibrating for 45 seconds and then allowed to dry for 24 hours. Twenty-four hours after the casting, the samples were de-molded and dried in ambient and oven settings. Until the testing age was attained, specimens were ambiently cured at room temperature (25 °C and 75% relative humidity) (28 and 56 Days). However, for oven curing, the de-molded samples were held in the oven at a temperature of (60 °C for 24 hours) but then left at room temperature until the age of testing. For outdoor cured specimens, humidity and temperature management are not necessary. At 28 and 56 days old, AAC samples underwent compressive strength testing.

2.2 Methods

The resultant mix proportions, indicated in Table 2, were created to create a total of 12 concrete mixes so that the parameters chosen for this investigation covered all of the mix design's limitations. Because of that, the study's changeable parameters include the ratio of alkaline solution to binder, curing and GGCS.

2.2.1 Mechanical strength tests

To examine the mechanical features of AAC, three cubes ($150 \times 150 \times 150 \, \text{mm}$) and three cylinders ($100 \, \text{mm}$ diameter x 200 mm height), with three prisms ($500 \times 100 \times 100 \, \text{mm}$), were cast for each mix then evaluated for compressive, split tensile and flexural strength after 28 and 56 days of curing. Compressive including flexural strength testing was conducted by IS 516:1959 [8] (or ASTM C78), whilst split tensile tests were carried out by IS 5816: 1999 [9], (or ASTM C496). The AAC's flexure strength is evaluated using the three-point loading test.

2.2.2 Creation of statistical models utilizing the response surface approach

This research examined the combined impact of flyash and GGCS on behavior of the cast-in-situ alkaliactivated concrete to establish a connection between input factors and output responses. The most potent combinations are discovered through the numerical optimization, which also decreases water absorption. The response surface analysis used a unique sequence of predictors to demonstrate statistical correlations among results with independent variables. Given that it can be employed when there are two independent variables, the central composite model was the most extensively applied with a reliable model [31, 37-41].

Design expert software was used for the experimental design. The cast in-situ alkali-activated concrete mix design formulas were randomly chosen for the two independent variables using a face-centered central composite design (FCCD). Flyash percentages ranging from 0 to 100% and GGCS percentages ranging from 10 to 50% by weight of the flyash were the design parameters examined. The results of this experiment included increases in compression strength, split tensile strength, flexural strength and overall weight decrease. For each response, the computer-generated five randomly duplicated combinations totaling thirty. The software uses the five duplications to compare the experiment's accuracy to any possible defects.

2.2.3 Field emission scanning electron microscopy

On a field emission scanning electron microscope equipped with EDAX (ULTRA plus, Carl Zeiss), the interfacial transition zone of concrete examples (20 mm in length, 20 mm in width and 25 mm in height) was investigated. Before testing, the samples' surfaces were coated with Au/Pd to make them conductive. Unreacted nanoparticles and cracks, including bonding among the aggregate and then paste, were all studied in the microstructures. Variations in elemental composition were mapped using EDAX from one location to the next.

3 Results and discussion

3.1 Compressive strength

The AAC compressive strength is determined by various parameters, including the binder content, alkaline content and aggregate used in the mix. Several trial mixes were created and tested. Two mixes were chosen based on the outcomes of the experiments. Figures 3-5 display the compressive strength of AAC at various ages (28 and 56 days) and the liquid-to-binder ratio (0.35, 0.40 and 0.45). With an increase in GGCS concentration in the mix, the compressive strength of both ambient and oven-cured AAC was increased. The presence of calcium was crucial in achieving AAC strength, which was further improved by producing C-A-S-H gels. After 28 days, ambient and oven-cured F70S30 samples have compressive strengths of 50.55 MPa and 53.77 MPa, correspondingly.

3.2 XRD analysis

The XRD is an important method used for cement concrete samples' quantitative and qualitative analysis. Here, pan analytical equipment is utilized. By using the XRD test results, a graph between the angle at which the wave was diffracted and intensity of X-Ray was

m D76 saibaba, kondraivendhan

determined. The XRD test was conducted on samples on the 28-th day. Figures 15-18 show XRD for AAC samples cured at ambient and oven conditions for 28 days for the mix F70S30. The diffractometer having a wavelength $\chi=1.54 \rm{\mathring{A}}$ at the scan step time [s] = 72.97. Scan Axis is $20-\omega$, start position, end position, step size, scan step time for 2θ is 10.0126, 99.9856, 0.0130, 72.9710 and scan type is continuous.

Some dissolvable minerals, such as quartz and mullite, have survived in all products, as evidenced by face-cantered XRD patterns. The peak (between 26° and 30°) in the fly ash and GGCS-based AAC XRD patterns indicates that the geopolymer material has semi-crystalline and amorphous structures. The peak (between 26° and 30°) in the reaction products with relatively lower intensities indicates that the alkaliactivated material has an almost completely amorphous structure.?? It was discovered that the alkali activators in both regimes have a diffuse hump between 26° and 30°. When partial replacement of fly ash with GGCS (20% and 30%) in ambient conditions was compared to the patterns of both grades, no significant change in AAC was detected.

3.3 Effect of curing on compressive strength

This study examined the AAC's compressive strength in relation to the impacts of ambient plus oven curing. Oven-cured samples get a greater compressive strength than ambient-cured samples. The strength gain is more significant since the polymerization procedure is frequently accelerated at a temperature greater than ambient. When it comes to casting in place, it is critical to cure at room temperature. High strength gains for F70S30, when exposed to ambient curing, is around 50.55 MPa, whereas the strength gains for F70S30, when exposed to oven curing, is around 53.35 MPa for 8M. With the addition of GGCS, ambient curing yielded satisfactory results without needing oven curing. As a result, oven curing can be avoided if AAC is manufactured with GGCS instead of fly ash. There was a quick rise in compressive strength up to 7 days after increasing the GGCS concentration in the mix and changing the liquid-to-binder ratio and the strength continued to improve up to 28 days. A blend with a 30% GGCS content in the overall binder composition provides more strength than a mix with a 50% GGCS content. The addition of calcium causes the strength of fly ash and GGCS-based AAC to increase. Including soluble calcium increases compressive strength, which speeds up the hardening process.

3.4 Effect of age on the strength of concrete

The connection between 7-day strength with 28-day strength is crucial for AAC. The study is also being

done to determine how strong AAC is after 28 and 56 days. The liquid-to-binder concentration, alkaline activator solution molarity and curing regime have the most considerable effects on the compressive strength of AAC. After 28 days of healing, oven-cured samples have an advanced compressive strength with respect to the ambient-cured ones. The strength of the oven-cured sample is roughly two times that of the ambient-cured specimen after 28 and 56 days of curing.

The early strength was quite active after seven days, while the later strength gain was reduced. The initial curing temperature influences the polymerization process. The amount of heating is crucial in increasing the strength of AAC, regardless of the concrete composition. Strength improvements happen more quickly at an early age than they do later. It was seen with both types of curing. However, oven-cured AAC exhibits a better growth in strength than the ambient curing. The early rate of strength progress within 28 days is substantial, but the strength gain was not as noticeable later as it is in typical concrete. The 28-day compressive strength to 56-day compressive strength ratio illustrates this. This ratio varied for samples that were ambiently cured from 1.04 to 1.35. In an oven-cured sample, the compressive strength ratio at 28 days to the compressive strength at 56 days ranged from 1.06 to 1.32. It unequivocally demonstrates that, compared to regular concrete, which has a ratio of 1.50, acquiring compressive strength beyond 28 days is extremely slow.

Additionally, a 2-dimensional plot was used to graphically illustrate the contour plot of the developed model, as seen in Figure 6. All the contour lines represented the optimal interaction between the GGCS and the curing regime. The independent variables in the model demonstrate complete synergy with one another. In the contour plot, the yellowish and greenish regions denote a fantastic combination that results in the best strength values. According to the three-dimensional surface diagram in Figure 6 the ambient cured, alkaliactivated mixes' compressive strength was raised and the setting time was shortened by adding GGCS to the mixtures. The presence of GGCS in the binder has a massive impact on the setting time of the pastes, causing them to harden more quickly since the model includes significant quantities of calcium oxide.

3.5 Split tensile strength

Figures 7-10 display the ambient, as well as the oven-cured specimens at the ages of 28 and 56 days. For Mix F90S10 - F50S50, the split tensile strength of AAC after 28 days was in the range of 2.25-4.80 MPa for ambient and oven curing, individually. It demonstrates that simple curing of the AAC specimens outside at average temperature is sufficient to achieve split tensile strength. It is owing to the geopolymer gel's tight connection with the aggregate particle. The split tensile

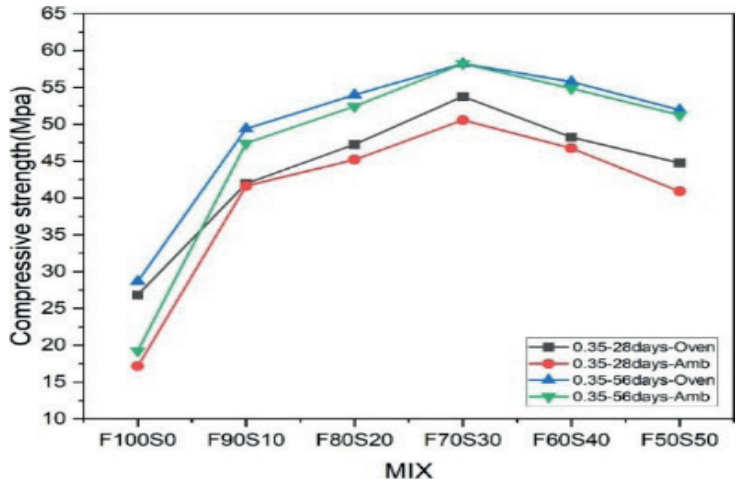
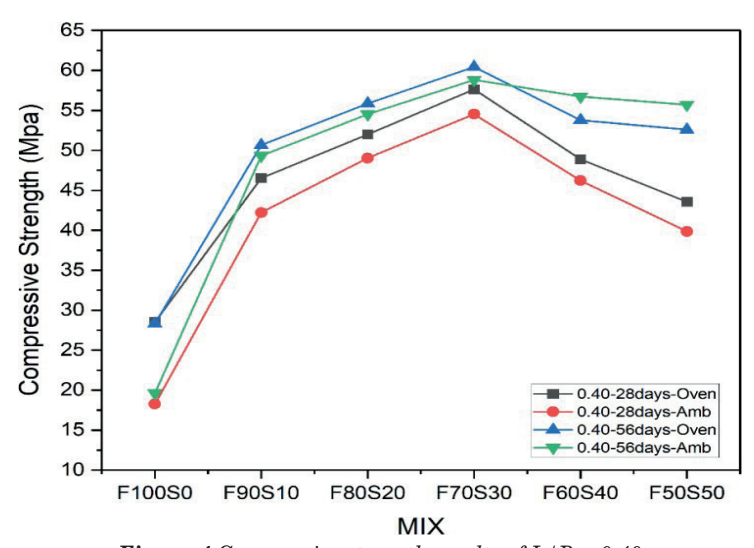
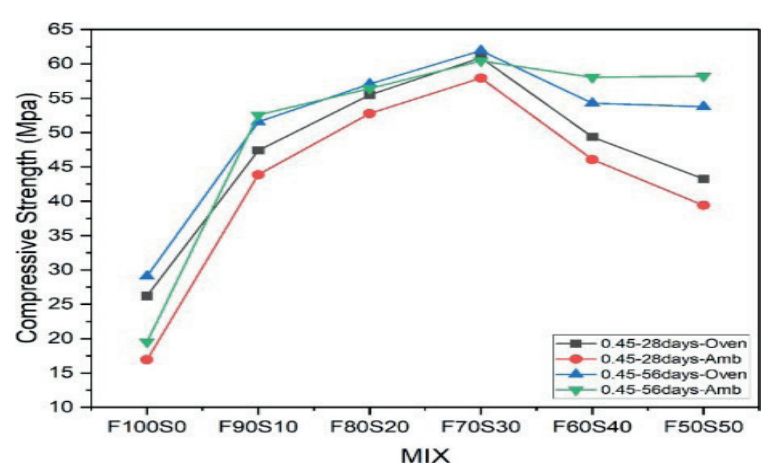


Figure 3 Compressive strength results of L/B = 0.35



 $\textbf{\it Figure 4} \ Compressive \ strength \ results \ of \ L/B = 0.40$

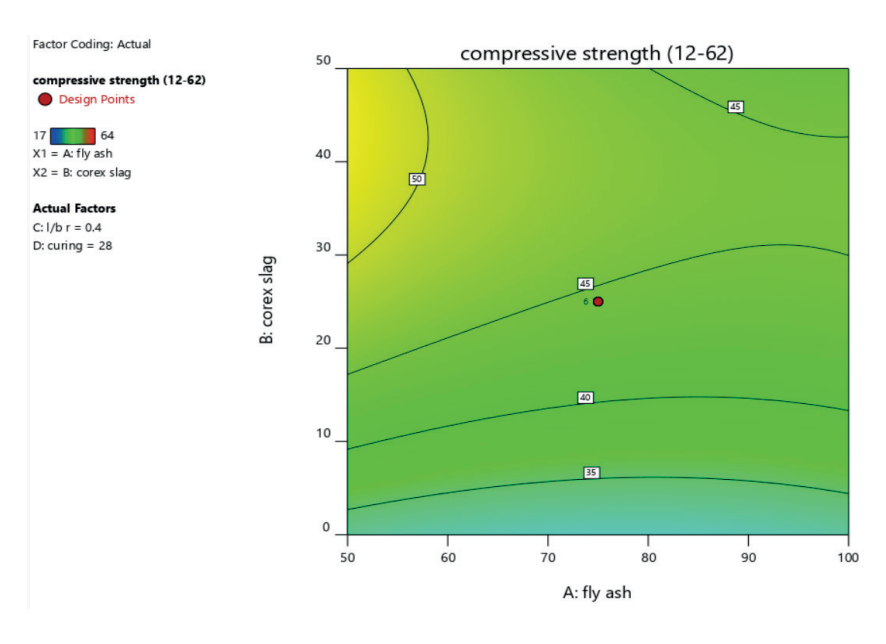


 $\textbf{\it Figure 5} \ Compressive \ strength \ results \ of \ L/B = 0.45$

strength of AAC samples treated under atmospheric temperatures rose to a satisfactory level with the calculation of GGCS for fly ash to the combination [22]. The material's tensile strength grew as the GGCS content did. Speculate that the rise in AAC strength is due to the continual creation of N-A-S-H and C-A-S-H gels. An empirical equation was established for ambient

and oven curing using the experimentally obtained compressive and splitting tensile strength values of fly ash and GGCS-based concrete, as shown in Equations (1) and (2), respectively. The connection between the compressive and tensile strengths in conventional concrete is 0.7 * $f_{\rm ck}$, but this value is lower when compared to traditional concrete.

D78 saibaba, kondraivendhan



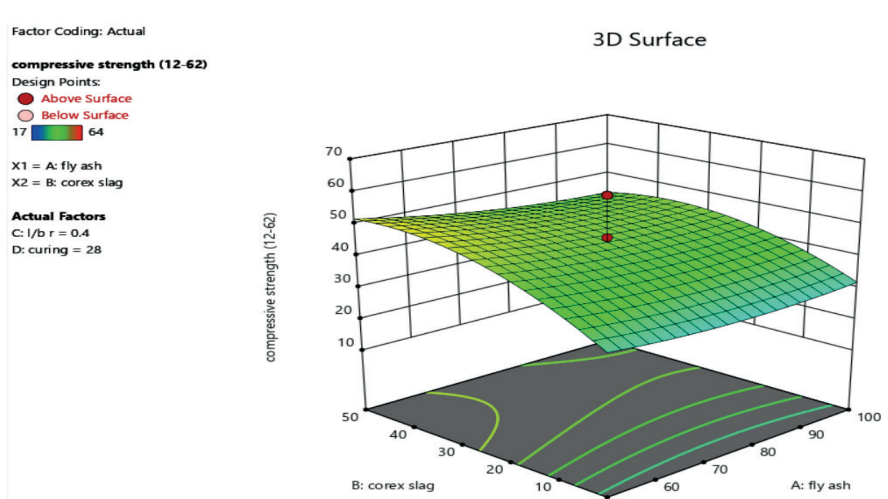


Figure 6 2-D and 3-D response surface diagram for compressive strength

$$Fsplit = 0.338 * \sqrt{fck} - ambient curing$$
 (1)

$$Fsplit = 0.4178 * \sqrt{fck} - Oven curing$$
 (2)

The splitting tensile strength is fsplit, while the Characteristic strength is fck.

3.6 Flexural strength

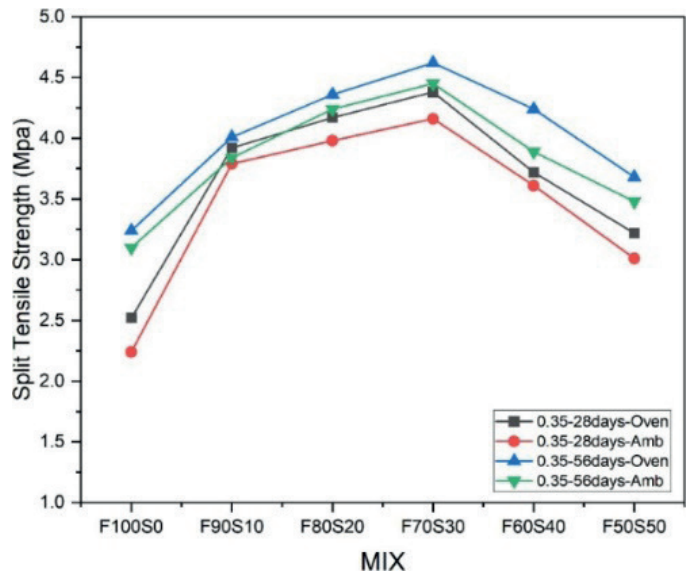
The flexural strength of the oven-cured specimens is superior to ambient-cured samples because of the quick polymerization process, as demonstrated in Figures 11 to 13. The flexural strength of ambient-cured AAC was 4.1 MPa, while that of oven-cured samples was 4.5 MPa. The flexural strength of AAC is increased as the GGCS content is improved. The GGCS component is essential for creating the C-A-S-H gel in the mix, increasing AAC

strength. The contribution of strength is due to this gel formation. Equations (3) and (4) show the relationship between the compressive and flexural strengths

$$Fsplit = 0.412 * \sqrt{fck} - ambient curing$$
 (3)

$$Fsplit = 0.437 * \sqrt{fck} - Oven \ curing \ . \tag{4}$$

The two-dimensional contour plots, presented in Figures 10 and 14, provide for precise observation of the change in splitting tensile with flexural strength across the mixes in the three-dimensional surface diagram (a). A yellowish area in Figures 10 and 14 represented the required variable combination. It demonstrates an excellent working relationship between the fly-ash and GGCS. The impact of the two factors (GGCS and other materials) on the split tensile strength with flexural strength after 28 days of ambient healing is depicted in a 3D dimensional diagram in Figures 10 and 14.



 $\textbf{Figure 7} \ Split \ tensile \ strength \ 0.35 \ liquid \ to \ binder \ ratio$

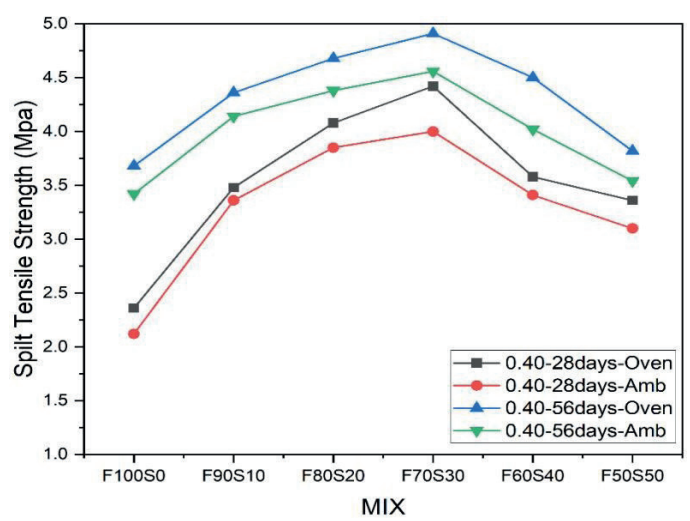
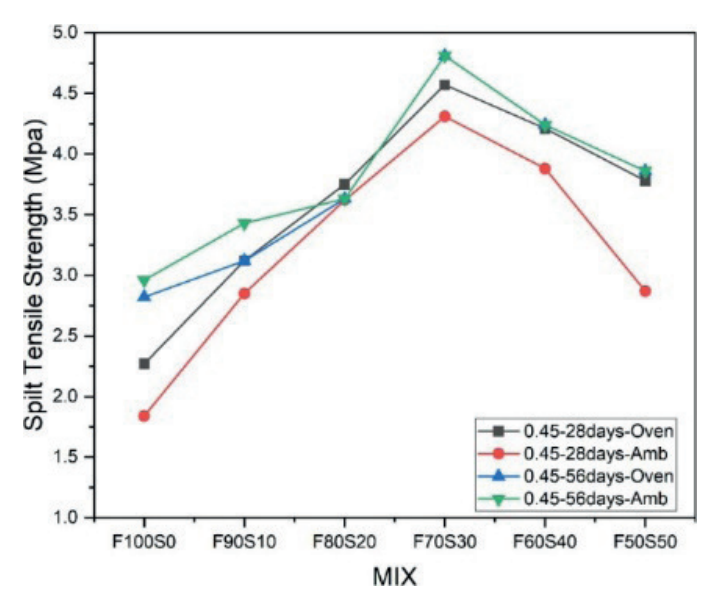


Figure 8 Split tensile strength 0.40 liquid to binder ratio



 $\textbf{\textit{Figure 9}} \ Split \ tensile \ strength \ 0.45 \ liquid \ to \ binder \ ratio$

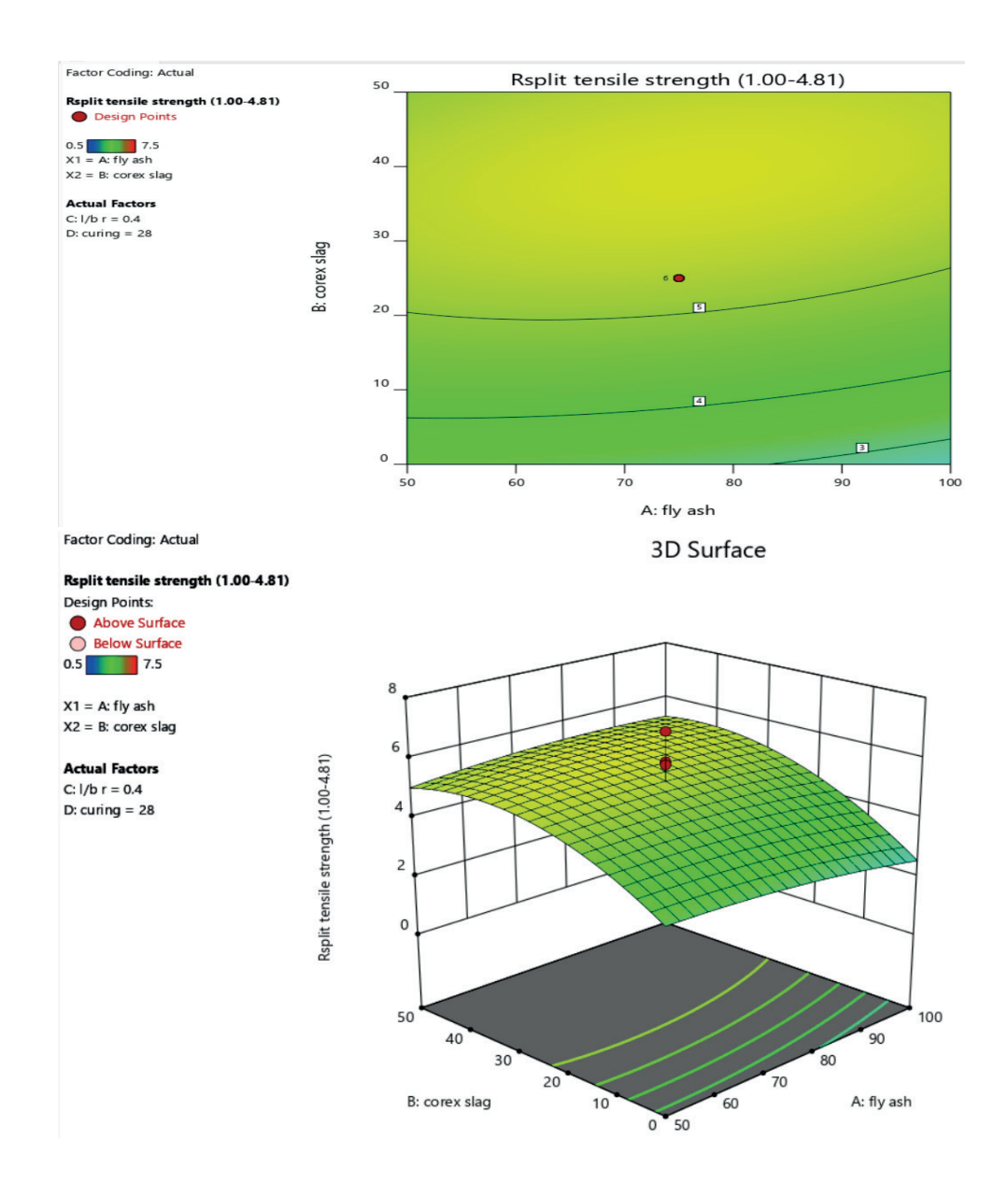


Figure 10 2-D and 3-D Response surface diagram for split tensile strength

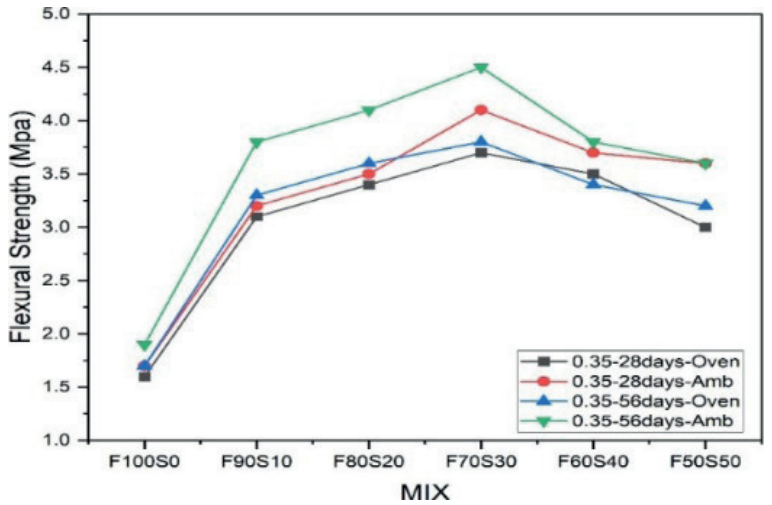


Figure 11 Flexural strength results of L/B = 0.35

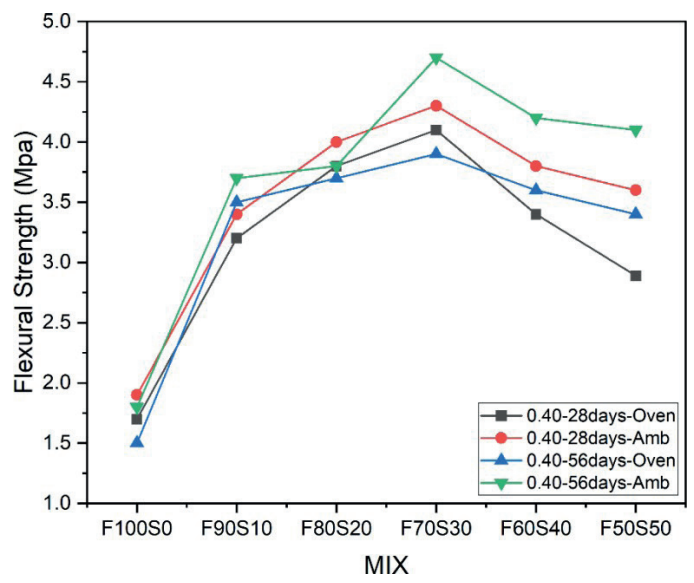


Figure 12 Flexural strength results of L/B = 0.40

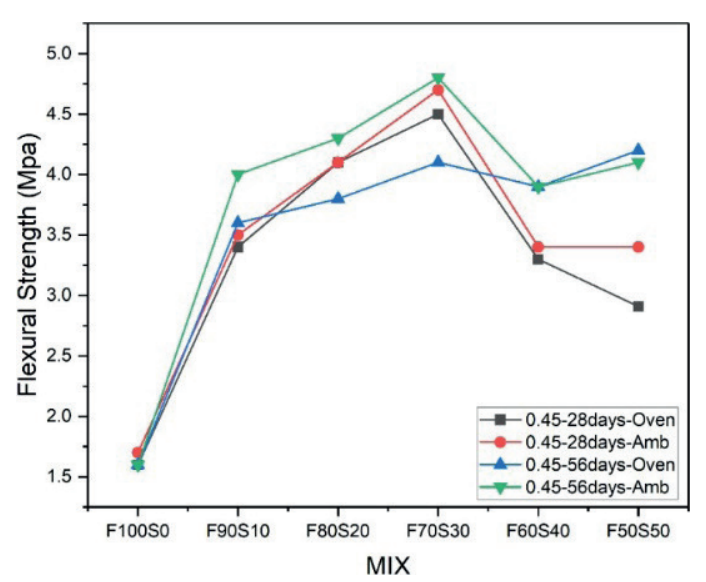


Figure 13 Flexural strength results of L/B = 0.45

3.7 SEM analysis

Using backscattered electron imaging, the AAC samples were analyzed. The fracture surfaces of materials, made using sodium silicate with sodium hydroxide solutions and cured in ambient as well as in an oven, respectively, are shown in Figures 19-22. The materials are heterogeneous and contain a significant amount of unreacted fly ash, as shown by the micrographs. A notable change in how the matrix-forming phases looked was seen for various curing regimes. The fly ash spheres were embedded in a glass-like matrix in the sample of ambiently cured silicate, while in the sample of oven-cured silicate, a composite matrix, made up of some glass-like and other more crystalline areas, had formed. Using micrographs of the fly ash activated in [4] to compare these pictures demonstrates that in this study, prolonged room-temperature procuring caused many fly ash dissolution and a continuous matrix phase

to develop. It helped the AAC materials to become more homogeneous, which was advantageous.

3.8 Interpretation of the test results using statistics

Each of the existing models has undergone statistical analysis and validation. To determine the relevance of experimental factors, the analysis was done at a level of 5%. Flexural strength, splitting tensile strength and compressive strength were the dependent variables in this experiment. In addition, the independent parameters Flyash, GGCS, liquid-to-binder ratio and curing regime were used. The resulting p-values in Tables 4-6 demonstrate that each factor was significant at a 95% level and was regarded as a critical factor in the test's outcome.

The regression coefficient (R2) value was utilized

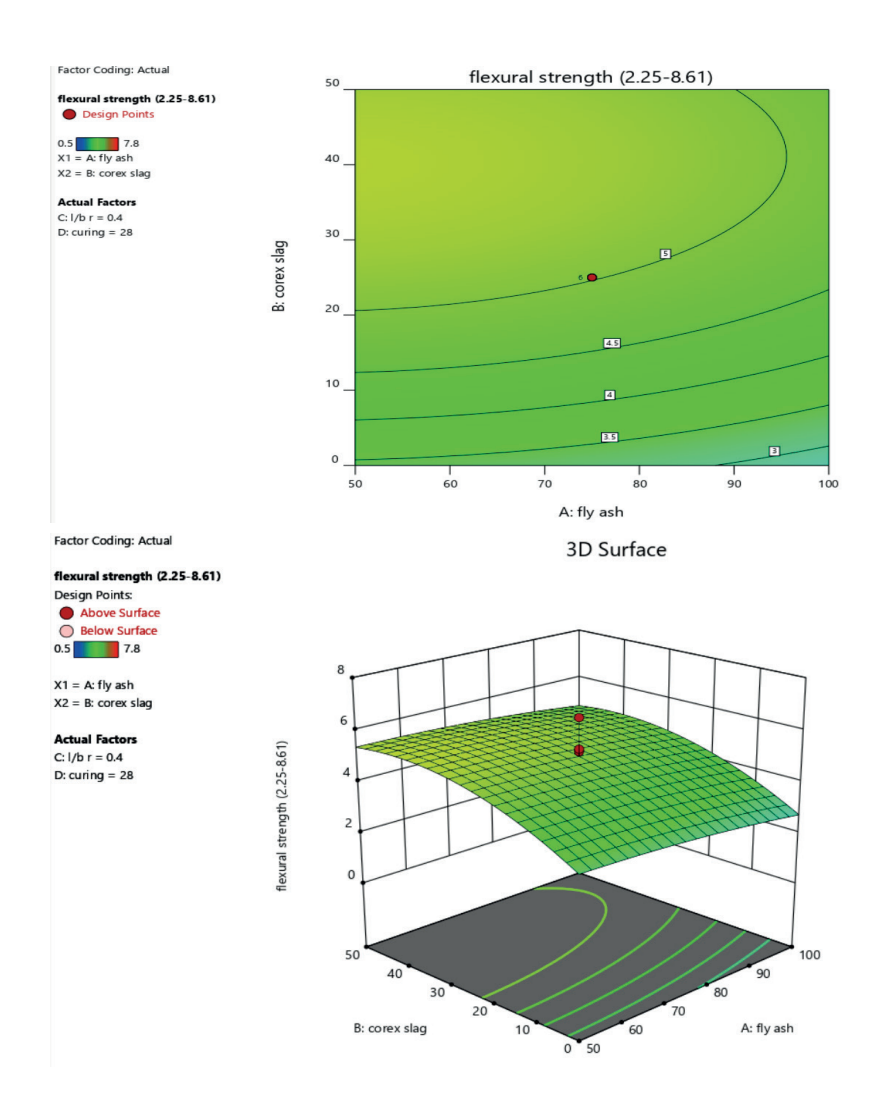


Figure 14 2-D and 3-D response surface diagram for flexural strength

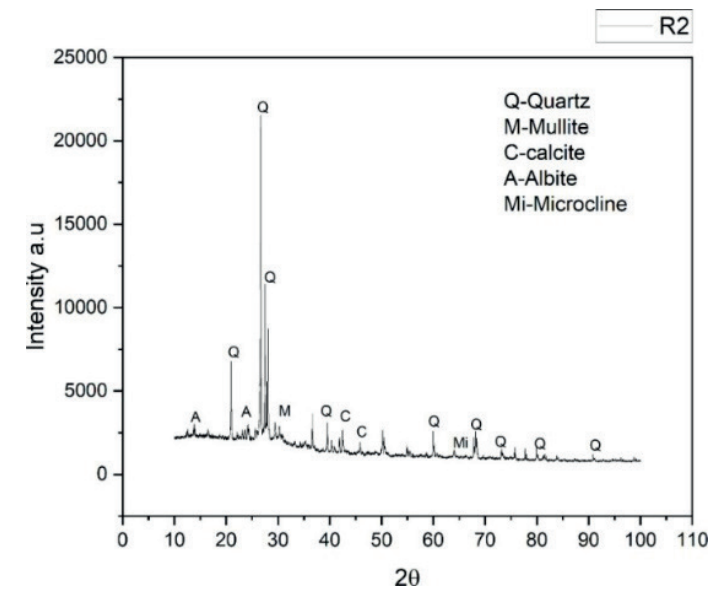


Figure 15 XRD Mix F70S30 0.35 L/B Ambient

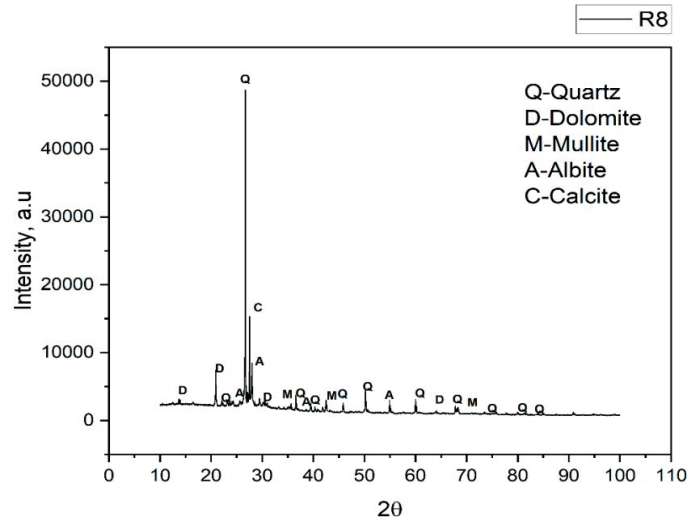


Figure 16 XRD Mix F70S30 0.45 L/B Ambient

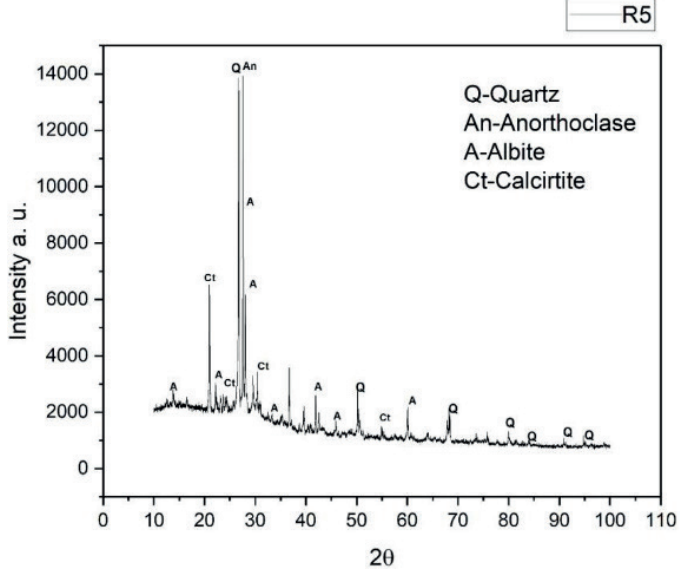


Figure 17 XRD Mix F70S30 0.35 L/B Oven

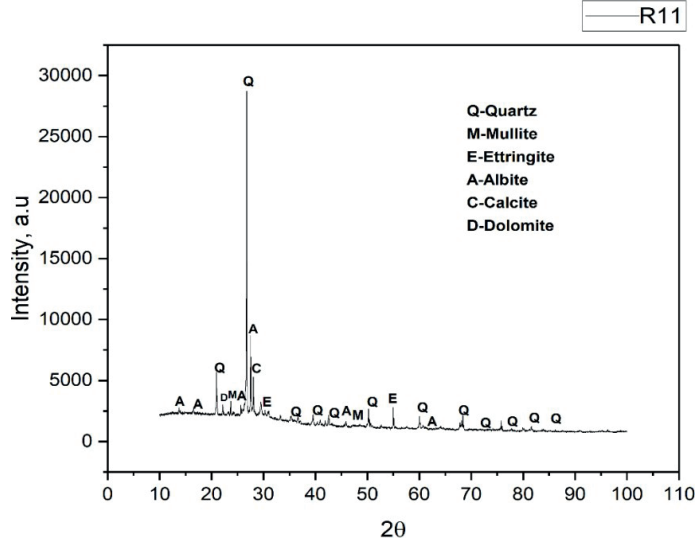


Figure 18 XRD Mix F70S30 0.45 L/B Oven

D84 SAIBABA, KONDRAIVENDHAN

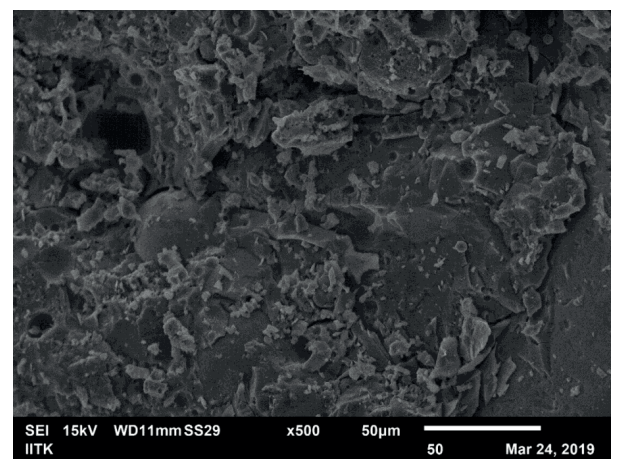


Figure 19 SEM Mix F70S30 0.35 L/B Oven

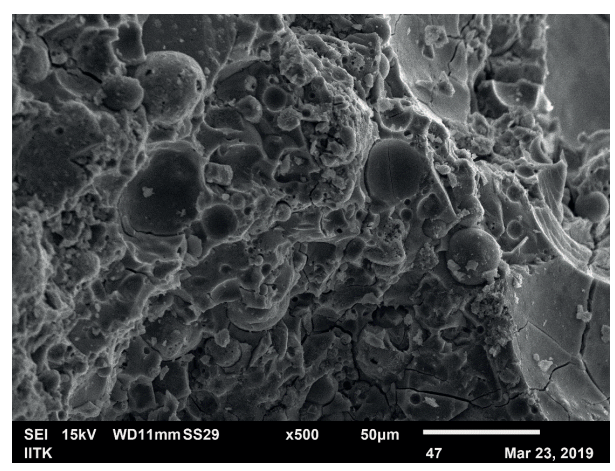


Figure 21 SEM Mix F70S30 0.45 L/B Oven

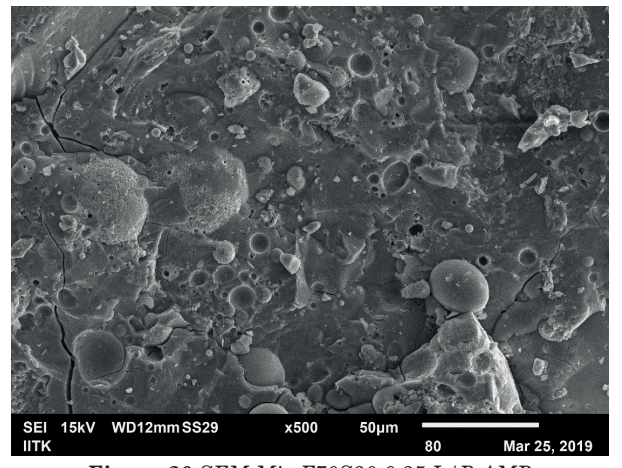


Figure 20 SEM Mix F70S30 0.35 L/B AMB

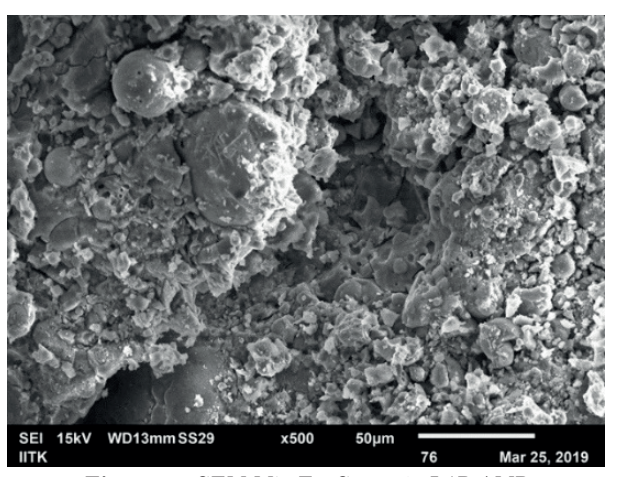


Figure 22 SEM Mix F70S30 0.45 L/B AMB

to evaluate the model's quality as can be shown in Tables 4-6, the models for compressive strength and split tensile strength. Flexural strength has high R2 values of 0.9947, 0.9925 and 0.9949, respectively, indicating excellent agreement between the projected and experimental data.

It is also important to note that there is less than 0.1 difference between the anticipated and adjusted R2 values, indicating agreement. As shown in Table 7, all of the models had enough precision values greater than 4, suggesting that they might be utilized to explore the solution space. The lack of fit can also be used to judge a model's quality; a lower value for the lack of fit implies a model that is worthier. Interestingly, all models' lack of fit P- values were significant, as shown in Tables 4-6, indicating high fitness for all the model answers.

To evaluate the data distribution and ensure that it is suitable, a standard probability plot is a form of a graph that is utilized [35, 42]. Figure 23 illustrates the normal distribution of the data for all residual responses by the virtually straight-line-like distribution of the points for all dependent variables. The competency and suitability of the modelling techniques were graphically evaluated by plotting the projected vs actual outcomes. The projected vs. actual results plot in Figure 23

show how the anticipated response model predicted the outcomes. The seamless fit of the data points to a straight line demonstrates a good correspondence between experimental findings and predictions made by the models in use. Since the cast in-situ alkali-activated concrete has various strengths, the existing response models were relevant and adequate in determining those strengths. However, an ANOVA approach may be used to predict the compressive strength of the cast-in-situ concrete, as demonstrated in Equation (1). Each response model was quadratic. Through the variance analysis, relationships and influences between variables and responses were established. These relationships are shown in Equation (8).

 $Compressive strength = 34.00 + 2.67A - \\ -0.6667B + 0.1667C + 12.82D + 0.25AB - \\ -0.125AC + 0.75AD + 0.125BC + 0.5BD - \\ -0.375CD + 0.1458A2 - 0.3542B2 + 0.0208C2 + \\ +0.6458D2$ (5)

$$Split\ tensil\ strength = 2.74 + 0.14A + 0.015B + \\ + 0.0841C + 1.17D + 0.1888AB - 0.1201AC + \\ + 0.0049AD + 0.1649BC - 0.151BD + 0.1013CD + \\ + 0.0121A2 + 0.0746B2 + 0.0346C2 - 0.0367D2$$
 (6)

 $Flexural\ strenght = 4.65 + 0.2362A + 0.2054B - \\ -0.1954C + 1.69D + 0.0056AB + 0.0731AC - \\ -0.1381AD - 0.0319BC - 0.0031BD + 0.0994CD + \\ +0.0047A2 - 0.0266B2 - 0.0128C2 + 0.1984D2.$ (7)

3.9 Optimization and validation study

To improve the strengths of the proposed concrete mixes, quantitative multi-objective optimization was

utilized to establish the proper GGCS and liquidto-binder ratio. Establishing desirable values for independent variables is the aim of optimization research to reach the optimization objectives. The RSM approach, which identifies the desired result's relevance purpose, was used to boost the replies that were affected by the numerous elements [32, 41]. The outcomes of numerical optimization solutions, based on the optimization objective, are shown in Table 8. The design expert program produced the ideal mixture fractions by combining 25% of GGCS with 0.4% of the

Table 4 Compressive strength

Factor	SS	DF	M.S	F-Value	P-Value	Remark
Model	4168.80	14	297.77	201.50	< 0.0001	Significant
A-Flyash	170.67	1	170.67	115.49	< 0.0001	
B-GGCS	10.67	1	10.67	7.22	0.0169	
C-L/B	0.6667	1	0.6667	0.4511	0.5120	
D-Curing	3952.67	1	3952.67	2674.74	< 0.0001	
AB	1.0000	1	1.0000	0.6767	0.4236	
\mathbf{AC}	0.2500	1	0.2500	0.1692	0.6867	
AD	9.00	1	9.00	6.09	0.0261	
BC	0.2500	1	0.2500	0.1692	0.6867	
BD	4.00	1	4.00	2.71	0.1207	
$^{\mathrm{CD}}$	2.25	1	2.25	1.52	0.2362	
A2	0.5833	1	0.5833	0.3947	0.5393	
B2	3.44	1	3.44	2.33	0.1479	
C2	0.0119	1	0.0119	0.0081	0.9297	
D2	11.44	1	11.44	7.74	0.0139	
Residual	22.17	15	1.48			
Lack of Fit	20.17	10	2.02	5.04	0.0441	Significant

Table 5 Split tensile strength

Factor	SS	DF	M.S	F-Value	P-Value	Remark
Model	34.82	14	2.49	138.09	< 0.0001	significant
A-fly ash	0.4279	1	0.4279	23.76	0.0002	
B-corex slag	0.0049	1	0.0049	0.2741	0.6088	
C-l/b r	0.1544	1	0.1544	8.57	0.0110	
D-curing	29.69	1	29.69	1648.57	< 0.0001	
AB	0.4960	1	0.4960	27.54	0.0001	
\mathbf{AC}	0.2006	1	0.2006	11.13	0.0049	
AD	0.0003	1	0.0003	0.0188	0.8928	
BC	0.3785	1	0.3785	21.01	0.0004	
BD	0.3133	1	0.3133	17.39	0.0009	
$^{\mathrm{CD}}$	0.1428	1	0.1428	7.93	0.0137	
A^2	0.0040	1	0.0040	0.2211	0.6454	
\mathbb{B}^2	0.1515	1	0.1515	8.41	0.0116	
C^2	0.0326	1	0.0326	1.81	0.2000	
D^2	0.0366	1	0.0366	2.03	0.1760	
Residual	0.2522	14	0.0180			
Lack of Fit	0.2429	9	0.0270	14.54	0.0044	significant

D86 SAIBABA, KONDRAIVENDHAN

Table 6 Flexural Strength

	_					
Factor	SS	DF	M.S	F-Value	P-Value	Remark
Model	73.96	14	5.28	207.06	< 0.0001	Significant
A-fly ash	1.34	1	1.34	52.51	< 0.0001	
B-corex slag	1.01	1	1.01	39.70	< 0.0001	
C-l/b r	0.9165	1	0.9165	35.92	< 0.0001	
D-curing	68.92	1	68.92	2701.46	< 0.0001	
AB	0.0005	1	0.0005	0.0198	0.8898	
AC	0.0856	1	0.0856	3.35	0.0870	
AD	0.3053	1	0.3053	11.97	0.0035	
BC	0.0163	1	0.0163	0.6372	0.4372	
BD	0.0002	1	0.0002	0.0061	0.9387	
$^{\mathrm{CD}}$	0.1580	1	0.1580	6.19	0.0251	
A^2	0.0006	1	0.0006	0.0236	0.8799	
B^2	0.0194	1	0.0194	0.7586	0.3975	
C^2	0.0045	1	0.0045	0.1765	0.6804	
D^2	1.08	1	1.08	42.34	< 0.0001	
Residual	0.3827	15	0.0255			
Lack of Fit	0.3577	10	0.0358	7.15	0.0212	significant

Table 7 Qualities that make a response model valid

Response	Compressive strength (MPa)	Split tensile strength (MPa)	Flexural strength(MPa)
Standard deviation	1.22	0.1342	0.1597
Mean	34.37	2.83	4.78
Coefficient of variation (CV %)	3.54	4.74	3.34
\mathbb{R}^2	0.9947	0.9928	0.9949
Predicted \mathbb{R}^2	0.9716	0.9538	0.9718
Adjusted R^2	0.9898	0.9856	0.9900
Adequate precision	59.71	48.34	60.016

Table 8 Optimization benchmark

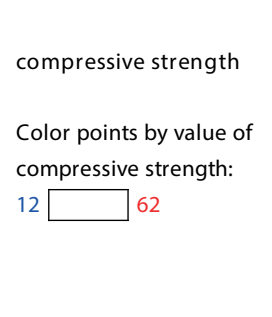
Factor and Responses	Target	Minimum value	Maximum Value
Flyash	In range	50	100
GGCS	In range	0	50
L/B ratio	In range	0.35	0.45
Curing	Type	28	60
Compressive Strength	Maximize	12	62
Split tensile strength	Maximize	1	4.81
Flexural Strength	Maximize	2.25	8.61

liquid-to-binder ratio. Improved responses with an 80% united desirability were attained. the second series of experiments were conducted utilizing the ideal mixture proportions with two other distinct mixes to assess the optimized combination percentage within the design mixes, the applicability of the results obtained and the overall response modelling. Table 9 provides an overview of the optimization criteria. Using Equation (4), the difference between experimental and anticipated values

was assessed and reported as a percentage, as seen in Table 9.

The optimization benchmark for the proposed methodology is displayed in Table 8. Table 8 displays the factors and responses for various attributes: the target, minimum and maximum value.

The average probability curve of the developed models is displayed in Figure 23. The normal percentage probability is shown on the Y-axis, while the X-axis



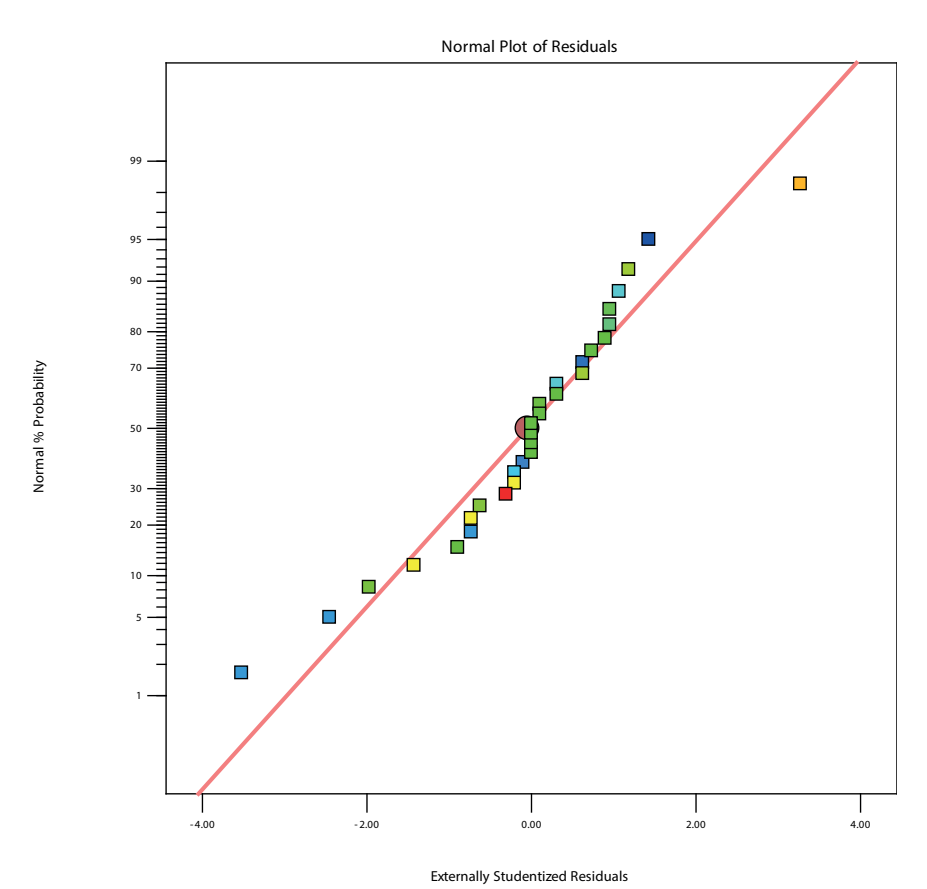


Figure 23 Normal probability plot of the developed models

Color points by value of compressive strength:

12 62

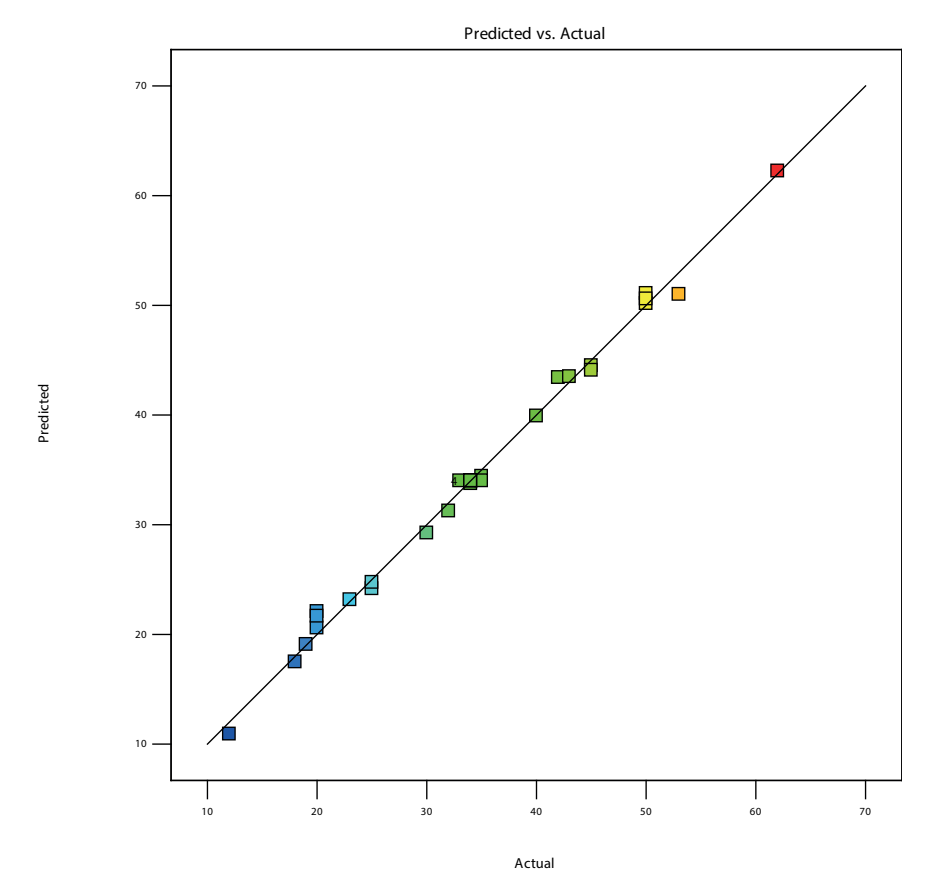


Figure 24 Predicted vs actual plot of the developed models

D88 saibaba, kondraivendhan

Table 9 Model verification

Responses	Liquid Binder ratio	GGCS	Predicted Outcomes	Experimental outcome	Error(%)
	0.35	50	49.15	51.95	5.39
Compressive strength	0.40	30	58.26	60.44	3.61
	0.45	10	50.18	52.56	4.53
Split tensile strength	0.35	50	3.51	3.68	4.62
	0.40	30	4.76	4.91	3.05
	0.45	10	2.78	2.96	6.08
Flexural strength	0.35	50	3.38	3.6	6.11
	0.40	30	4.43	4.7	5.74
	0.45	10	3.85	4	3.75

displays the externally studentized residuals.

The derived models' projected vs the actual plot is displayed in Figure 24. The actual values are shown on the X-axis and the predicted values for our proposed approach are shown on the Y-axis.

$$Error(\%) = \frac{Experimental\ value - predicted\ value}{Experimental\ value} * 100\%$$
. (8)

4 Conclusions

This work has intended to characterize and improve the cast-in-situ alkali-activated concrete using the response surface approach. The scientific results of this investigation allow for the following deductions:

Since the strength gains of 24.5% and 18.6% were attained at 28 and 56 days, respectively, the strength gain of the cast-in-situ alkali-activated concrete was identical to that of the regular Portland cement. Strength growth is significantly increased when the GGCS replaces fly ash to a greater extent. However, as shown by the microstructural investigation, adding GGCS to the binder induces structural aluminosilicate changes in the in-situ alkali-activated concrete that has been created. The alterations were connected to the source materials'

reactive alumina and silica polymerization.

The quadratic nature of all the response models suggests a strong correlation between the factors and thereplies.

The RSM optimization study's findings reveal that adding 25% GGCS and a 0.40 liquid-to-binder ratio to the total weight of the critical materials led to the optimum strengths.

The experimental data and the predictions showed a strong correlation. The results of the validation were quite similar to the measured data.

Grants and funding

The author received no financial support for the research, authorship and/or publication of this article.

Conflicts of interest

The author declare that they have no known competing financial interests or personal relationships that could have appeared to influence the work reported in this paper.

References

- [1] HARDJITO, D., RANGAN, B. V. Development and properties of low-calcium fly ash-based geopolymer concrete. Research Report GC 1. Perth, Australia: Faculty of Engineering, Curtin University of Technology, 2005.
- [2] FLATT, R. J., ROUSSEL, N., CHEESEMAN, C. R. Concrete: an eco-material that needs to be improved. Journal of the European Ceramic Society [online]. 2012, 32(11), p. 2787-2798. ISSN 0955-2219. Available from: https://doi.org/10.1016/j.jeurceramsoc.2011.11.012
- [3] COLLINS, F., SANJAYAN, J. G. Cracking tendency of development and properties alkali-activated slag concrete subjected to restrained shrinkage. Cement and Concrete Research [online]. 2000, 30(5), p. 791-798. ISSN 0008-8846, eISSN 1873-3948. Available from: https://doi.org/10.1016/S0008-8846(00)00243-X
- [4] VORA, P. R., DAVE, U. V. Parametric studies on compressive strength of geopolymer concrete. *Procedia Engineering* [online]. 2013, **51**, p. 210-219. ISSN 1877-7058. Available from: https://doi.org/10.1016/j.proeng.2013.01.030
- [5] WALLAH, S., RANGAN, B. V. Low-calcium fly ash-based geopolymer concrete: long-term properties. Research Report GC 2. Perth, Australia: Faculty of Engineering, Curtin University of Technology, 2006.

- [6] PACHECO-TORGAL, F., CASTRO-GOMES, J., JALALI, S. Alkali-activated binders: a review: Part 1. Historical background, terminology, reaction mechanisms and hydration products. *Construction and Building Materials* [online]. 2008, 22(7), p. 1305-1314. ISSN 0950-0618, eISSN 1879-0526. Available from: https://doi.org/10.1016/j.conbuildmat.2007.10.015
- [7] WHITING, J. Manufacture of cement. US Patent No. 544,706. 1895.
- [8] DAVIDOVITS, J. Geopolymers: inorganic polymeric new materials. Journal of Thermal Analysis and Calorimetry [online]. 1991, 37(8), p. 1633-1656. ISSN 1388-6150, eISSN 1588-2926. Available from: https://doi.org/10.1007/ BF01912193
- [9] NEUPANE, K. Fly ash and GGBFS based powder-activated geopolymer binders: a viable sustainable alternative of portland cement in concrete industry. *Mechanics of Materials* [online]. 2016, 103, p. 110-122. ISSN 0167-6636, eISSN 1872-7743. Available from: https://doi.org/10.1016/j.mechmat.2016.09.012
- [10] HARUNA, S., MOHAMMED, B. S., SHAHIR-LIEW, M., ALALOUL, W. S., HARUNA, A. Effect of water-binder ratio and NaOH molarity on the properties of high calcium fly ash geopolymer mortars at outdoor curing. *International Journal of Civil Engineering and Technology (IJCIET)*. 2018, 9(10), p. 1339-1352. ISSN 0976-6308, eISSN 0976-6316.
- [11] HAJIMOHAMMADI, A., VAN DEVENTER, J. S. Characterization of one-part geopolymer binders made from fly ash. Waste and Biomass Valorization [online]. 2017, 8(1), p. 225-233. ISSN 1877-2641, eISSN 1877265X. Available from: https://doi.org/10.1007/s12649-016-9582-5
- [12] DAVIDOVITS, J. The manufacture of geopolymer cements. In: *Geopolymer chemistry and applications*. DAVIDOVITS, J. 4. ed. Saint-Quentin, France: Geopolymer Institute, 2015. ISBN 978-2951482098, p. 499-521.
- [13] VAN DEVENTER, J. S. J., PROVIS, J. L., DUXSON, P. Technical and commercial progress in the adoption of geopolymer cement. *Minerals Engineering* [online]. 2012, 29, p. 89-104. ISSN 0892-6875, eISSN 1872-9444. Available from: https://doi.org/10.1016/j.mineng.2011.09.009
- [14] SARKER, P. K., HAQUE, R., RAMGOLAM, K. V. Fracture behaviour of heat cured fly ash based geopolymer concrete. *Materials and Design* [online]. 2013, 44, p. 580-586. ISSN 0264-1275. Available from: https://doi.org/10.1016/j.matdes.2012.08.005
- [15] MOHAMMED, B. S., ACHARA, B. E., NURUDDIN, M. F., YAW, M., ZULKEFLI, M. Z. Properties of nano-silica-modified self-compacting engineered cementitious composites. *Journal of Cleaner Production* [online]. 2017, 162, p. 1225-1238. ISSN 0959-6526, eISSN 1879-1786. Available from: https://doi.org/10.1016/j.jclepro.2017.06.137
- [16] MOHAMMED, B. S., FANG, O. C., HOSSAIN, K. M. A., LACHEMI, M. Mix proportioning of concrete containing paper mill residuals using response surface methodology. *Construction and Building Materials* [online]. 2012, 35, p. 63-68. ISSN 0950-0618, eISSN 1879-0526. Available from: https://doi.org/10.1016/j.conbuildmat.2012.02.050
- [17] YAO, Z. T., XIA, M. S., SARKER, P. K., CHEN, T. Z. A review of the alumina recovery from coal fly ash, with a focus in China. Fuel [online]. 2014, 120, p. 74-85. ISSN 0016-2361, eISSN 1873-7153. Available from: https://doi.org/10.1016/j.fuel.2013.12.003
- [18] CHATTERJEE, A. K. Technological initiatives and status of fly ash in India. In: *Fly ash: sources applications and potential environmental impacts*. SARKER, P. K. (Ed.). USA: Nova, 2014. ISBN 978-1-62948-044-2, p. 315-359.
- [19] NEMATOLLAHI, B., SANJAYAN, J., SHAIKH, F. U. A. Synthesis of heat and ambient cured one-part geopolymer mixes with different grades of sodium silicate. *Ceramics International* [online]. 2015, 41(4), p. 5696-5704. ISSN 0272-8842, eISSN 1873-3956. Available from: https://doi.org/10.1016/j.ceramint.2014.12.154
- [20] SARKER, P. K. Analysis of geopolymer concrete columns. *Materials and Structures* [online]. 2009, 42(6),
 p. 715-724. ISSN 1359-5997, eISSN 1871-6873. Available from: https://doi.org/10.1617/s11527-008-9415-5
- [21] MERMERDAS, K., ALGIN, Z., OLEIWI, S. M., NASSANI, D. E. Optimization of lightweight GGBFS and FA geopolymer mortars by response surface method. *Construction and Building Materials* [online]. 2017, 139, p. 159-171. ISSN 0950-0618, eISSN 1879-0526. Available from: https://doi.org/10.1016/j.conbuildmat.2017.02.050
- [22] CHINDAPRASIRT, P., DE SILVA, P., SAGOE-CRENTSIL, K., HANJITSUWAN, S. Effect of SiO2 and Al2O3 on the setting and hardening of high calcium fly ash-based geopolymer systems. *Journal of Materials Science* [online]. 2012, 47(12), p. 4876-4883. ISSN 0022-2461, eISSN 1573-4803. Available from: https://doi.org/10.1007/s10853-012-6353-y
- [23] BERNAL, S., DE GUTIERREZ, R., DELVASTO, S., RODRIGUEZ, E. Performance of an alkali-activated slag concrete reinforced with steel fibers. *Construction and Building Materials* [online]. 2010, **24**(2), p. 208-214. ISSN 0950-0618, eISSN 1879-0526. Available from: https://doi.org/10.1016/j.conbuildmat.2007.10.027
- [24] PHOO-NGERNKHAM, T., MAEGAWA, A., MISHIMA, N., HATANAKA, S., CHINDAPRASIRT, P. Effects of sodium hydroxide and sodium silicate solutions on compressive and shear bond strengths of FA-GBFS geopolymer. *Construction and Building Materials* [online]. 2015, **91**, p. 1-8. ISSN 0950-0618, eISSN 1879-0526. Available from: https://doi.org/10.1016/j.conbuildmat.2015.05.001

D90 SAIBABA, KONDRAIVENDHAN

[25] OUELLET-PLAMONDON, C., HABERT, G. Life cycle assessment (LCA) of alkali-activated cements and concretes. In: *Handbook of alkali-activated cements, mortars and concretes* [online]. PACHECO-TORGAL, F., LABRINCHA, J., LEONELLI, C., PALOMO, A., CHINDAPRASIT, P. (Eds.). Woodhead Publishing Elsevier, 2015. ISBN 978-1-78242-276-1, p. 663-686. Available from: https://doi.org/10.1016/C2013-0-16511-7

- [26] RAO, G. M., RAO, T. D., SESHU, R. D., VENKATESH, A. Mix proportioning of geopolymer concrete. *Cement Wapno Beton* [online]. 2016, 21(4), 274. ISSN 1425-8129.
- [27] THUNUGUNTLA, C. S., GUNNESWARA RAO, T. D. Mix design procedure for alkali-activated slag concrete using particle packing theory. *Journal of Materials in Civil Engineering* [online]. 2018, **30**(6), 04018113. ISSN 0899-1561, eISSN 1943-5533. Available from: https://doi.org/10.1061/(ASCE)MT.1943-5533.0002296
- [28] PROVIS, J. L. Alkali-activated materials. Cement and Concrete Research [online]. 2018, 114, p. 40-48. ISSN 0008-8846, eISSN 1873-3948. Available from: https://doi.org/10.1016/j.cemconres.2017.02.009
- [29] MOHAMMED, B. S., KHED, V. C., NURUDDIN, M. F. Rubber crete mixture optimization using response surface methodology. *Journal of Cleaner Production* [online]. 2018, 171, p. 1605-1621. ISSN 0959-6526, eISSN 1879-1786. Available from: https://doi.org/10.1016/j.jclepro.2017.10.102
- [30] SARKER, P. K. Bond strength of reinforcing steel embedded in fly ash-based geopolymer concrete. *Materials and Structures* [online]. 2011, 44(5), p. 1021-1030. ISSN 1359-5997, eISSN 1871-6873. Available from: https://doi.org/10.1617/s11527-010-9683-8
- [31] MONTGOMERY, D. C. Design and analysis of experiments. John Wiley and Sons, 2019. ISBN 978-1-119-49244-3.
- [32] MTARFI, N. H., RAIS, Z., TALEB, M., KADA, K. M. Effect of fly ash and grading agent on the properties of mortar using response surface methodology. *Journal of Building Engineering* [online]. 2017, **9**, p. 109-116. eISSN 2352-7102. Available from: https://doi.org/10.1016/j.jobe.2016.12.004
- [33] MOHAMMED, B. S., LIEW, M. S., ALALOUL, W. S., AL-FAKIH, A., IBRAHIM, W., ADAMU, M. Development of rubberized geopolymer interlocking bricks. *Case Studies in Construction Materials* [online]. 2018, **8**, p. 401-408. eISSN 2214-5095. Available from: https://doi.org/10.1016/j.cscm.2018.03.007
- [34] MOHAMMED, B. S., ADAMU, M. Mechanical performance of roller compacted concrete pavement containing crumb rubber and nano silica. *Construction and Building Materials* [online]. 2018, **159**, p. 234-251. ISSN 0950-0618, eISSN 1879-0526. Available from: https://doi.org/10.1016/j.conbuildmat.2017.10.098
- [35] ZAHID, M., SHAFIQ, N., ISA, M. H., GIL, L. Statistical modeling and mix design optimization of fly ash based engineered geopolymer composite using response surface methodology. *Journal of Cleaner Production* [online]. 2018, **194**, p. 483-498. ISSN 0959-6526, eISSN 1879-1786. Available from: https://doi.org/10.1016/j.jclepro.2018.05.158
- [36] SIYAL, A. A., AZIZLI, K. A., MAN, Z., ISMAIL, L., KHAN, M. I. Geopolymerization kinetics of fly ash based geopolymers using JMAK model. *Ceramics International* [online]. 2016, **42**(14), p. 15575-15584. ISSN 0272-8842, eISSN 1873-3956. Available from: https://doi.org/10.1016/j.ceramint.2016.07.006
- [37] BALA, N., NAPIAH, M., KAMARUDDIN, I. Nanosilica composite asphalt mixtures performance-based design and optimization using response surface methodology. *International Journal of Pavement Engineering* [online]. 2020, **21**(1), p. 29-40. Available from: https://doi.org/10.1080/10298436.2018.1435881
- [38] BALA, N., KAMARUDDIN, I., NAPIAH, M., SUTANTO, M. H. Polymer nanocomposite-modified asphalt: characterization and optimization using response surface methodology. *Arabian Journal for Science and Engineering* [online]. 2019, 44(5), p. 4233-4243. ISSN 2193-567X, eISSN 2191-4281. Available from: https://doi.org/10.1007/s13369-018-3377-x
- [39] MOHAMMED, B. S., KHED, V. C., LIEW, M. S. Optimization of hybrid fibres in engineered cementitious composites. *Construction and Building Materials* [online]. 2018, **190**, p. 24-37. ISSN 0950-0618, eISSN 1879-0526. Available from: https://doi.org/10.1016/j.conbuildmat.2018.08.188
- [40] MOHAMMED, B. S., ADAMU, M. Evaluating the static and dynamic modulus of elasticity of roller compacted rubber crete using response surface methodology. *International Journal of GEOMATE* [online]. 2018, **14**(41), p. 186-192. Available from: https://doi.org/10.21660/2018.41.42833
- [41] ANDERSON, M. J., WHITCOMB, P. J. RSM simplified: optimizing processes using response surface methods for design of experiments [online]. 2. ed. New York: Productivity Press, 2016. ISBN 9781315382326. Available from: https://doi.org/10.1201/9781315382326
- [42] MOHAMMED, B. S., LIEW, M. S., ALALOUL, W. S., AL-FAKIH, A., IBRAHIM, W., ADAMU, M. Development of rubberized geopolymer interlocking bricks. *Case Studies in Construction Materials* [online]. 2018, 8, p. 401-408. Available from: https://doi.org/10.1016/j.cscm.2018.03.007